Superexchange-Driven Magnetoelectricity in Magnetic Vortices

Kris T. Delaney,[1] Maxim Mostovoy,[2] and Nicola A. Spaldin[1]

[1]*Materials Department, University of California, Santa Barbara, California 93106-5050, USA*
[2]*Zernike Institute for Advanced Materials, University of Groningen, Nijenborg 4, The Netherlands*

(Received 17 October 2008; published 17 April 2009)

We demonstrate that magnetic vortices in which spins are coupled to polar lattice distortions via superexchange exhibit an unusually large linear magnetoelectric response. We show that the periodic arrays of vortices formed by frustrated spins on kagome lattices provide a realization of this concept; our *ab initio* calculations for such a model structure yield a magnetoelectric coefficient that is 30 times larger than that of prototypical single phase magnetoelectrics. Finally, we identify the design rules required to obtain such a response in a practical material.

DOI: 10.1103/PhysRevLett.102.157203 PACS numbers: 75.80.+q, 71.15.Mb, 75.25.+z, 75.30.Et

The ability to control magnetism with electric fields, which can be realized through the interplay between spins and charges in solids, has an obvious technological appeal. The simplest form of such control is the linear magnetoelectric effect, in which an antiferromagnet in an electric field **E** acquires a magnetization **M**, while an applied magnetic field **H** induces an electric polarization **P**, both proportional to the field:

$$P_i = \alpha_{ij} H_j, \qquad M_j = \alpha_{ij} E_i. \tag{1}$$

Here α_{ij} is the magnetoelectric tensor, and summation over repeated indices is implied. This magnetoelectric response requires simultaneous breaking of inversion and time-reversal symmetries, which defines the allowed magnetic symmetry classes and the nonzero components of the magnetoelectric tensor. While the phenomenology of the linear magnetoelectric effect is now well understood [1,2], the use of magnetoelectrics is hampered by rather low values of their magnetoelectric constants: For example, in the prototypical magnetoelectric Cr_2O_3, a (large) electric field of 10^6 V/cm induces a (tiny) magnetization of $\sim 10^{-3}\mu_B$ per Cr ion [3]. The search for materials with stronger response requires new ideas about spin orders and crystal lattices that can conspire to produce a large magnetoelectric effect.

Two recent developments in the related field of multiferroics, which are materials with simultaneous ferroelectric and (ferro)magnetic order, underlie the work we present in this Letter. First, an early observation that spiral magnetic order can lead to an electrical polarization [4] has been confirmed repeatedly [5,6], and the list of such materials has been considerably enlarged. While spectacular nonlinear magnetoelectric effects, such as reorientation of electric polarization with a magnetic field, have been observed, the polarizations in such spiral magnets are small because they are induced by the weak spin-orbit-driven Dzyaloshinskii-Moriya interaction [7,8]. At the same time, a new class of multiferroics has been identified in which the magnetic ordering couples to the lattice through mechanisms of nonrelativistic origin, in particular, exchange striction arising from superexchange [9,10]. The stronger spin-lattice coupling leads to correspondingly larger magnetically induced ferroelectric polarizations, with polarization values close to those of conventional ferroelectrics. Here we show that these two concepts from the field of multiferroics—symmetry breaking in spiral magnets and superexchange-mediated spin-lattice coupling—can be combined to yield materials with a strong linear magnetoelectric response.

We begin by considering the magnetoelectric response of a single spin vortex [Fig. 1(a)]. This can be viewed as a magnetic spiral rolled into a circle, and so we use the following result [11] from spiral multiferroics to determine its magnetoelectric response: The electric polarization induced by rotating spins lies in the plane of the spiral and is orthogonal to its propagation vector. Then the polarization in a vortex is locally oriented in the radial direction. In zero magnetic field, when the rotation of spins is uniform, this yields zero net polarization [Fig. 1(a)]. A magnetic field applied in the xy plane leads to a nonuniform rotation of spins in the vortex, which results in a nonzero net electric polarization proportional to the magnetic field [see Fig. 1(b)]. The spin vortex shown in Fig. 1(a) has a diago-

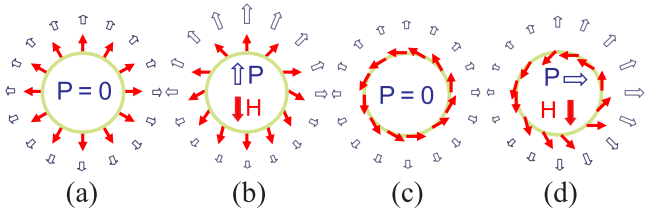

FIG. 1 (color online). (a) A magnetic vortex carrying a monopole moment. The thin solid arrows indicate the spin orientation, while the thick open arrows show the local polarization vector. (b) A magnetic field applied to the vortex shown in (a) induces a net polarization along the field direction. (c) A magnetic vortex with a toroidal moment. (d) A magnetic field applied to (c) induces an electric polarization perpendicular to the field.

nal magnetoelectric tensor, with magnetization induced parallel to the applied electric field, while for the vortex shown in Fig. 1(c), an applied magnetic field induces a perpendicular electric polarization and the magnetoelectric tensor is antisymmetric [see Fig. 1(d)] [12].

Next we analyze the spin-lattice coupling resulting from the dependence of the Heisenberg superexchange interaction between spins on their relative positions. Figure 2 shows a schematic diagram of a three-atom unit consisting of two magnetic transition-metal ions connected by a ligand, such as oxygen, that mediates superexchange. Because of charge differences, the cations and ligand shift in opposite directions under application of an electric field. The exchange constant coupling the spins depends on the amplitude of the relative shifts through the changes in the metal-oxygen distance and the metal-oxygen-metal bond angle θ. According to the Anderson-Kanamori-Goodenough rules [14], the exchange is antiferromagnetic ($J > 0$) for $\theta = 180°$ and ferromagnetic ($J < 0$) for $\theta = 90°$. Experiments varying A-site cation size in transition-metal oxides have shown that the crossover from ferromagnetic to antiferromagnetic coupling is continuous [15]. Therefore, the total magnetization of the unit can be modified by applying an electric field; conversely, changes in spin orientation will affect its electric dipole moment.

Now we combine these two concepts to form a periodic array of magnetic vortices in which the magnetic moments are coupled through superexchange and show that the combination leads to a large magnetoelectric response. The macroscopic magnetoelectric response of an array of magnetic vortices is proportional to the vortex density. Therefore we choose the smallest possible magnetic vortex as our building block: a triangle of antiferromagnetically coupled spins, in which the angle between spins in the lowest-energy state is 120° [Fig. 3(a)]. We use transition-metal (TM) ions to provide the spins and incorporate oxygen ligands between them for superexchange spin-spin interactions. Upon application of an electric field, the shifts of the oxygen anions relative to the positive TM ions induce changes in the Heisenberg exchange energy, canting the spins to result in a nonzero magnetization. The symmetry of the magnetoelectric response of the triangle is identical to that of the magnetic vortices of Fig. 1, with the form of the in-plane magnetoelectric tensor constrained by its C_3 symmetry to

$$\alpha_{ij} = -\alpha_0 \begin{pmatrix} \cos\varphi & \sin\varphi \\ -\sin\varphi & \cos\varphi \end{pmatrix}. \quad (2)$$

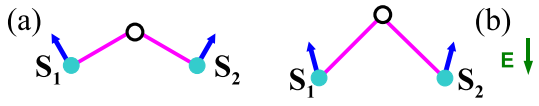

FIG. 2 (color online). (a) Two magnetic cations (solid circles) connected by a ligand (open circle). (b) Upon application of the electric field, the bond lengths and angle change resulting in a different relative alignment of spins $\mathbf{S}_1$ and $\mathbf{S}_2$.

Here φ is the angle between spins and the radial axis. In particular, $\varphi = 0$ [Fig. 3(a)] leads to $\alpha_{ij} = -\alpha_0\delta_{ij}$, so that for $\alpha_0 > 0$ the induced magnetization $\mathbf{M}$ is antiparallel to the electric field $\mathbf{E}$; for $\varphi = \pi/2$, $\mathbf{M}$ is perpendicular to $\mathbf{E}$ [Fig. 3(b)].

To transform the concepts outlined above into a model material with a three-dimensional periodic structure, we begin with planes of Mn atoms situated on the vertices of a kagome lattice and assume that their spins form the 120° structure with zero wave vector (Fig. 4), as observed, e.g., in iron jarosite $KFe_3(OH)_6(SO_4)_2$ [16]. This zero wave vector spin structure is stabilized by antiferromagnetic next-nearest-neighbor exchange interactions and magnetic anisotropies [17,18]. At first glance, such a spin lattice would yield no magnetoelectric response because spins in the vortices formed at "up" and "down" triangles are oriented in opposite senses ($\varphi = 0$ and $\varphi = \pi$). However, when oxygen ions are positioned outside the up triangles and inside the down triangles, the sign of the local magnetoelectric coupling [α_0 in Eq. (2)] also alternates and the contributions of all triangles to α_{ij} have the same sign. This can be understood by comparing the magnetoelectric response of the $\mathbf{S}_2$-$\mathbf{S}_1$ and $\mathbf{S}_1$-$\mathbf{S}_2'$ spin pairs and noting that, for fixed bond lengths and angle, only the scalar product of spins is important in Heisenberg exchange. This mechanism would produce no net magnetoelectric response in the case of kagome magnets with the so-called $\sqrt{3} \times \sqrt{3}$ spin structure, stabilized by ferromagnetic next-nearest-neighbor exchange [17], which contains equal numbers of $\phi = 0$, $2\pi/3$, and $-2\pi/3$ triangles.

The two-dimensional plane shown in Fig. 4 has a similar structure to the MnO layers of the experimentally realized $YMnO_3$ structure [19], which consists of a connected mesh of oxygen trigonal bipyramids with Mn atoms at their centers. Using this structure as motivation, we extend our two-dimensional MnO planes to a model three-dimensional crystal and introduce counterions (Ca and

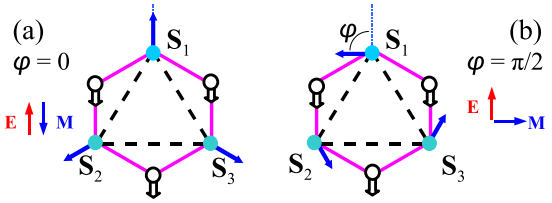

FIG. 3 (color online). Magnetoelectric response of a single spin triangle. Antiferromagnetic coupling of $\mathbf{S}_1$, $\mathbf{S}_2$, and $\mathbf{S}_3$ (solid arrows) leads to a 120° spin order (zero magnetization) in the classical ground state. For $\varphi = 0$ (a), all spins are oriented out from the center of the triangle analogous to Fig. 1(a). In an applied electric field $\mathbf{E}$, the oxygen atoms (open circles) displace (open arrows) relative to TM ions (solid circles) inducing a magnetization through changes in the exchange coupling. The magnetization $\mathbf{M}$ is opposite in direction to $\mathbf{E}$ for $\varphi = 0$, regardless of the orientation of $\mathbf{E}$. For $\varphi = \frac{\pi}{2}$ (b), the spin triangle has a toroidal moment [Fig. 1(c)], and the induced magnetization is perpendicular to the electric field.

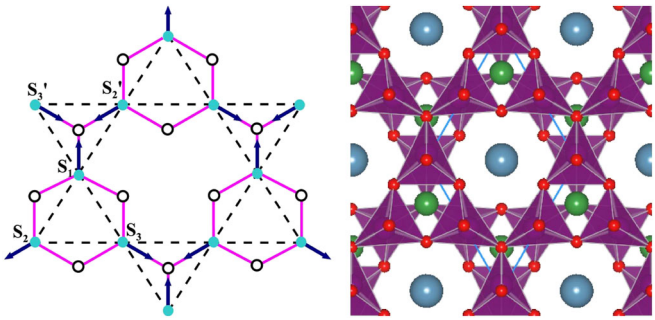

FIG. 4 (color online). (Left) The structure of one MnO plane. The Mn atoms (solid circles) are arranged on a kagome lattice (dashed lines) with oxygen atoms (open circles) mediating the binding and superexchange. (Right) Two layers of KITPite in the zero-field structure (space group *Pmma*). The Mn ions are at the center of the oxygen trigonal bipyramids (purple polyhedra). The correct charge balance is obtained through Ca (blue) and Al (green) counterions in voids of the MnO mesh.

Al) in the voids of the lattice so that the correct charge balance is attained. To ensure that the sign of magnetoelectric response is the same for all layers, the neighboring MnO planes are rotated by 180° with respect to each other (Fig. 4). This reverses the positioning of oxygen ions with respect to the up and down spin triangles in the next layer, which compensates the reversal of the spin direction that must result from the antiferromagnetic interlayer coupling provided by the 180° connections through the apical oxygen atoms. Our resulting "KITPite" structure [20], with chemical formula $CaAlMn_3O_7$, correctly breaks I and T symmetry; in addition, the apical oxygen ions between the MnO layers are centers of combined IT symmetry.

We first estimate the magnetoelectric response of the model material using a simple analytic approach in which only oxygen ions displace with respect to the rest of the lattice under application of an electric field. By considering the geometry of the MnO planes with spin-spin coupling provided by Heisenberg superexchange, we obtain, after some algebra,

$$\alpha = \frac{SQ\mu_B J'}{JK\nu}, \tag{3}$$

where $S = 2$ is the spin of the Mn ions, $Q = 2e$ is the nominal charge of oxygen ions, and μ_B is the Bohr magneton. J and J' describe the nearest-neighbor spin-exchange constant and its derivative with respect to symmetric oxygen shifts, respectively. K is the spring constant, and ν is the volume per Mn ion. From the dependence of J on the Mn-O bond length and the Mn-O-Mn bond angle [21], we get $J'/J \sim 3.5$ Å^{-1}. The frequency of the polar phonon mode in hexagonal manganites [22] (≈ 300 cm^{-1}) allows us to estimate $K \sim 6$ eV Å^{-2}, and we take $J \sim 3$ meV [23]. Using these data and Eq. (3), we obtain $\alpha \approx 10^{-3}$ for the dimensionless magnetoelectric constant.

Finally, we calculate the magnetoelectric constant from first principles using plane-wave density-functional theory as implemented in VASP [24]. We use projector-augmented wave potentials for core-valence separation [25] and include noncollinear magnetism for the valence electrons. We approximate the exchange-correlation part of the Kohn-Sham potential using the rotationally invariant form of the LSDA + U in the fully localized limit [26], with the Hubbard U applied only to the Mn d electrons ($U = 5.5$ eV and $J = 0.5$ eV [27]). It is important to note that we deliberately do not include spin-orbit coupling in our calculations to ensure that the obtained magnetoelectric constant arises entirely from the superexchange coupling. As a result, the monopole and toroidal spin arrangements [Figs. 3(a) and 3(b)] are degenerate.

We first relax the structure in the absence of an electric field by optimizing the ionic coordinates to find the lowest-energy state with the constraint that the trigonal bipyramids are prevented from tilting; this ensures a locally stable lattice structure while preserving the kagome structure of the MnO planes and does not impede the lattice mode responsible for magnetoelectricity. The resulting structure is shown in Fig. 4. Our calculated valence electronic structure is, as expected, similar to that of $YMnO_3$ [19]: The effective Mn charge is close to the nominal $3+$, with four d electrons per Mn adopting a high-spin configuration with local moment $\sim 4\mu_B$/Mn.

Subsequently, we apply an electric field and calculate the linear response of the ions [28]. The force on an ion in an external electric field is determined by the Born effective charge tensor $Z^\star$ through $F_{\mu i} = Z^\star_{\mu ij} E_j$, where $\mathbf{F}$ is the force, $\mathbf{E}$ is the applied electric field, μ is an index denoting the ion, and i and j are spatial directions. All elements of the $Z^\star$ tensor are computed through derivatives of the bulk polarization $Z^\star_{\mu ij} = \frac{\delta P_j}{\delta R_{\mu i}}$, where $\mathbf{P}$ is calculated using the Berry-phase approach [29] for a small displacement in all degrees of freedom individually.

In order to obtain the first-order ionic response to the field, we use the force-constant matrix $C_{\mu i,\nu j} = \frac{\delta F_{\mu i}}{\delta R_{\nu j}}$. Then, to linear order, the ionic displacements for a given electric field are found through the inverted force-constant matrix $\delta R_{\nu j} = C^{-1}_{\nu j,\mu i} Z^\star_{\mu ik} E_k$. Finally, the total magnetization is calculated as a function of E_k.

Figure 5 shows the calculated magnitude of the induced magnetization as a function of applied electric field. With a field of 10^6 V/cm, the ionic response leads to an average relative displacement between Mn and O atoms of 0.012 Å parallel to the field. The Born effective charges $Z^\star$ have an in-plane average magnitude of $+3.30e^-$ for Mn and $-2.26e^-$ for O. Applying $E = 10^6$ V/cm along the direction of S_1 (Fig. 4), the spins S_2 and S_3 rotate by $-0.1°$ and $0.1°$, respectively, leading to a magnetoelectric coupling coefficient of $\alpha = 1.22 \times 10^{-5}$ J T^{-1} V^{-1} m^{-2}. Transformation to Gaussian units yields $\alpha_G = 3.66 \times 10^{-4}$, close to the analytic estimate. For a benchmark, we compare to the magnetoelectric response of Cr_2O_3 computed also within density-functional theory [28,30]

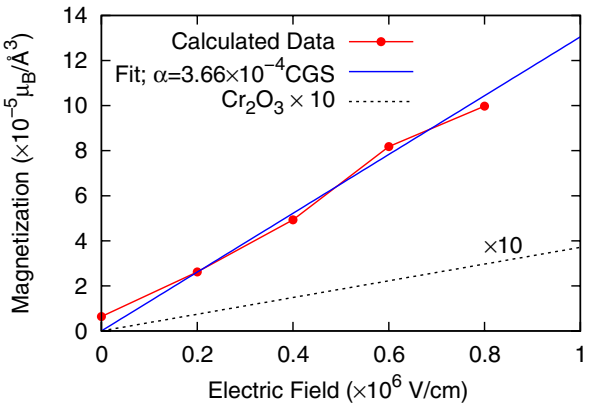

FIG. 5 (color online). Calculated magnetoelectric response of the model system using density-functional theory and a linear fit.

$\alpha_G(Cr_2O_3) = 1.0 \times 10^{-5}$ (in good agreement with the experimental value at $T = 0$). Hence, our model system has a magnetoelectric coupling around 30 times larger than that of Cr_2O_3. Since spin-orbit coupling was not considered in this work, the magnetoelectric coupling is demonstrably driven by superexchange. As a side effect, magnetic anisotropies are absent so that we cannot predict φ of KITPite in the ground state. However, the strength of the superexchange magnetoelectric coupling [α_0 in Eq. (2)] is insensitive to φ.

In conclusion, we have combined the concepts of magnetically induced polarization in magnetic vortices with lattice-mediated coupling through superexchange to demonstrate strong magnetoelectric coupling in geometrically frustrated antiferromagnets. We showed that such a mechanism can be studied using modern density-functional theory approaches with noncollinear spin density functionals augmented with linear-response methods, and we explicitly calculated the magnetoelectric coupling of a model transition-metal oxide. While the linear magnetoelectric response of our model compound is relatively strong, we anticipate that many further improvements are possible: In particular, materials with larger polarizability through increased $Z^\star$'s or reduced rigidity would be promising. We hope that this study will stimulate the search for additional novel strongly coupled magnetoelectric materials.

This work was initiated during the research program on Moments and Multiplets in Mott Materials at the Kavli Institute for Theoretical Physics at UC Santa Barbara under NSF Grant No. PHY05-51164. K. T. D. and N. A. S. were supported by the NSF under Grant No. DMR-0605852. M. M. was supported by the Stichting voor Fundamenteel Onderzoek der Materie (FOM). Calculations were performed at the California Nanosystems Institute with facilities provided by NSF Grant No. CHE-0321368 and Hewlett-Packard, at SDSC, and at NCSA.

[1] L. D. Landau and E. M. Lifshitz, *Electrodynamics of Continuous Media* (Addison-Wesley, Reading, MA, 1960).
[2] M. Fiebig, J. Phys. D **38**, R123 (2005).
[3] D. N. Astrov, Sov. Phys. JETP **11**, 708 (1960).
[4] R. E. Newnham, J. J. Kramer, W. A. Schulze, and L. E. Cross, J. Appl. Phys. **49**, 6088 (1978).
[5] T. Kimura, T. Goto, H. Shintani, K. Ishizaka, T. Arima, and Y. Tokura, Nature (London) **426**, 55 (2003).
[6] T. Goto, T. Kimura, G. Lawes, A. P. Ramirez, and Y. Tokura, Phys. Rev. Lett. **92**, 257201 (2004).
[7] H. Katsura, N. Nagaosa, and A. V. Balatsky, Phys. Rev. Lett. **95**, 057205 (2005).
[8] I. A. Sergienko and E. Dagotto, Phys. Rev. B **73**, 094434 (2006).
[9] I. A. Sergienko, C. Sen, and E. Dagotto, Phys. Rev. Lett. **97**, 227204 (2006).
[10] S. Picozzi, K. Yamaguchi, B. Sanyal, I. A. Sergienko, and E. Dagotto, Phys. Rev. Lett. **99**, 227201 (2007).
[11] M. Mostovoy, Phys. Rev. Lett. **96**, 067601 (2006).
[12] These conclusions are independent of the magnetoelectric coupling mechanism and are determined only by the symmetry. The vortices shown in Figs. 1(a) and 1(c) have, respectively, a monopole moment $A \propto \sum_\alpha \mathbf{r}_\alpha \cdot \mathbf{S}_\alpha$ and a toroidal moment $\mathbf{T} \propto \sum_\alpha \mathbf{r}_\alpha \times \mathbf{S}_\alpha$. See Ref. [13].
[13] N. A. Spaldin, M. Fiebig, and M. Mostovoy, J. Phys. Condens. Matter **20**, 434203 (2008).
[14] P. W. Anderson, *Magnetism* (Academic Press, New York, 1963), Vol. 1.
[15] M. A. Subramanian, A. P. Ramirez, and W. J. Marshall, Phys. Rev. Lett. **82**, 1558 (1999).
[16] D. Grohol, K. Matan, J.-H. Cho, S.-H. Lee, J. W. Lynn, D. G. Nocera, and Y. S. Lee, Nature Mater. **4**, 323 (2005).
[17] A. B. Harris, C. Kallin, and A. J. Berlinsky, Phys. Rev. B **45**, 2899 (1992).
[18] M. Elhajal, B. Canals, and C. Lacroix, Phys. Rev. B **66**, 014422 (2002).
[19] B. B. Van Aken, T. T. M. Palstra, A. Filippetti, and N. A. Spaldin, Nature Mater. **3**, 164 (2004).
[20] After the Kavli Institute for Theoretical Physics, where this structure was first suggested by the authors.
[21] L. E. Gontchar and A. E. Nikiforov, Phys. Rev. B **66**, 014437 (2002).
[22] M. N. Iliev *et al.*, Phys. Rev. B **56**, 2488 (1997).
[23] T. J. Sato *et al.*, Phys. Rev. B **68**, 014432 (2003).
[24] G. Kresse and J. Furthmüller, Phys. Rev. B **54**, 11 169 (1996).
[25] G. Kresse and D. Joubert, Phys. Rev. B **59**, 1758 (1999).
[26] A. I. Liechtenstein, V. I. Anisimov, and J. Zaanen, Phys. Rev. B **52**, R5467 (1995).
[27] Z. Yang, Z. Huang, L. Ye, and X. Xie, Phys. Rev. B **60**, 15 674 (1999).
[28] J. Íñiguez, Phys. Rev. Lett. **101**, 117201 (2008).
[29] R. D. King-Smith and D. Vanderbilt, Phys. Rev. B **47**, 1651 (1993).
[30] Note that the dimensionless α used in Ref. [28] is related to α_G used in this Letter by $\alpha = 4\pi\alpha_G$.